Journal of Fluids and Structures 39 (2013) 306–321

Contents lists available at SciVerse ScienceDirect

Journal of Fluids and Structures

journal homepage: www.elsevier.com/locate/jfs

Wind pressures on tapered and set-back tall buildings

Yong Chul Kim [a,*], Jun Kanda [b]

[a] Wind Engineering Research Center, Tokyo Polytechnic University, 1583 Iiyama, Atsugi, Kanagawa Prefecture 243-0297, Japan
[b] Graduate School of Frontier Sciences, The University of Tokyo, 5-1-5 Kashiwa-no-ha, Kashiwa, Chiba Prefecture 277-8563, Japan

ARTICLE INFO

Article history:
Received 25 April 2012
Accepted 3 February 2013
Available online 16 March 2013

Keywords:
Aerodynamic modification
Pressure coefficient
Cross-correlation coefficient
Power spectra
Co-coherence

ABSTRACT

Recent tall buildings tend to have irregular and unconventional shapes as a prevailing but unavoidable trend, which is very effective for suppressing across-wind responses. Suppression of across-wind responses is a major factor in safety and habitability design of tall buildings, and the so-called aerodynamic modification method is comprehensively used. While the effectiveness of aerodynamic modification in reducing wind loads has been widely reported, there have been few detailed investigations of pressure fluctuations. The purpose of the present work is to investigate the spatio-temporal characteristics of pressure fluctuations applied to height-modified tall buildings comprehensively, including differences of vortex formation and shedding mechanism based on the previously reported mechanism of a conventional square tall building. The results show that taper and set-back affect on the bandwidth of power spectra and position of peak frequencies. And through taper and set-back, the height at which the vortex begins to form moves up, and due to the small building dimension, the vortex component formed at that height sheds from the building more frequently before an inverted conical vortex is formed over the whole height.

1. Introduction

The current tallest building in the world is the 828 m-high Burj Khalifa, which is over 300 m higher than Taipei 101, and the tallest buildings in the next decade will be Kingdom Tower (over 1000 m), which will be completed in 2018, making Burj Khalifa the third tallest building (http://www.skyscrapercenter.com/List/future-tallest-100-buildings, 2012). Current trend of tall building construction, i.e., manhattanization with various building shapes, requires attention. Their free-wheeling building shapes are expressed by taper, set-back, helical, openings, or combinations of these, reflecting architects' and engineers' challenging spirits for new forms. These irregular and unconventional building shapes are a resurrection of an old characteristic, motivated by new trends in architecture, but they have the advantage of mitigating across-wind responses, which is a major factor in safety and habitability of tall buildings.

The effectiveness of aerodynamic modifications in reducing wind loads has been widely examined, and they can be tentatively classified as corner modification and height modification (Kim and Kanda, 2010a). Corner modification includes corner cut, recess, chamfer and addition of fins (Kawai, 1998; Kwok et al., 1988), and height modification includes taper, set-back, opening, helical (twisting) and inclined (tilted) shape, and so on (Dutton and Isyumov, 1990; Kim and Kanda, 2010a, 2010b; Kim et al., 2011; Tanaka et al., 2012). In particular, Tanaka et al. (2012) conducted a series of wind tunnel tests to investigate aerodynamic characteristics and to evaluate the most effective building shape in wind-resistant design for 31 tall buildings with various aerodynamic modifications. Unlike structural modification, which controls mass, spring and damping directly in a governing equation of motion, aerodynamic modification controls forces applied to tall buildings by altering the separated shear layer or disturbing the alignment of the vortex over the whole height.

* Corresponding author. Tel./fax: +81 46 242 9927.
E-mail addresses: kimyc@t-kougei.ac.jp, gentle95@gmail.com (Y.C. Kim).

0889-9746/$ - see front matter © 2013 Elsevier Ltd. All rights reserved.
http://dx.doi.org/10.1016/j.jfluidstructs.2013.02.008

However, most previous researches have focused on the results of mitigation effect in terms of wind forces (or local wind forces) and responses. And although many studies have been conducted to investigate the characteristics of pressure fluctuations, only the conventional building shapes with square/rectangular or circular cross-sections have been focused on the existing studies (Hui et al., 2013; Iungo et al., 2012; Kareem and Cermak, 1984; Lin et al., 2005; Okuda and Taniike, 1993). There have been few detailed investigations of pressure fluctuations, especially for the height-modified tall buildings. In the present work, the comprehensive spatio-temporal characteristics of pressure fluctuations on height-modified tall buildings including peak pressures, cross-correlations, power spectra and coherence were investigated through the synchronous multi-pressure sensing system techniques. The differences of vortex formations and shedding mechanisms were also investigated based on the previously reported vortex formation and shedding mechanism of a conventional square tall building. And, the effect of different flow conditions is examined from the variation of mean pressure coefficients and power spectral peaks.

2. Wind tunnel test

Wind tunnel tests were conducted in an Eiffel-type wind tunnel (1.8 m × 1.8 m × 12.5 m) at the University of Tokyo. Four tall building models were used: a prototype square prism (SQ), a building model with set-back at mid-height (SB), and two tapered building models with tapering ratios of 10% (TP1) and 5% (TP2). The bottom dimensions (B_B and D_B) were 40 m and the top dimensions (B_T and D_T) ranged from 24 m to 40 m depending on building shape, and the height (H) was 160 m in full scale. For all models, the side ratio was unity and the aspect ratio (H/B_B) was four (Fig. 1).

The models had 55 pressure taps on each surface connected to vinyl tubes 1.4 mm in inner diameter and 800 mm in length. The pressure taps were equally spaced horizontally at $D_h/5$ or $B_h/5$, and $D_h/10$ or $B_h/10$ from the edge of each surface, and vertically at $H/10$ and $H/20$ from the bottom and top. Here, H means total height of the models and h means any height of the models. Wind pressures were measured using a synchronous multi-pressure sensing system. The natural frequency of the piezoelectric transducer was about 1.7 kHz, and a low-pass filter of 500 Hz cutoff frequency was installed in each data acquisition channel to eliminate aliasing effects. In a run time, the reference differential pressure transducer was connected to a pitot-tube installed in the test section. The tubing effects were numerically compensated using the gain and phase shift characteristics of the pressure measurement system (Fig. 2).

Fig. 3 shows the definition of wind directions and location of pressure taps used in the present study. Pressure measurements were conducted in two ways: pressure measurement on one surface (Fig. 3(a)) and pressure measurement on opposite surfaces for the taps located at odd and even levels separately as shown in Fig. 3(b) and (c). Pressure measurement on one surface was conducted for wind directions from 0° to 180° at 15° intervals and pressure measurement on opposite surfaces was conducted for wind directions 0° and 90°. A sampling frequency was set to 1000 Hz, and the measuring time was adjusted such that over 40 samples were obtained. A length scale of 1/400 and a velocity scale of 1/70 were assumed, considering the design wind speed at 160 m in Tokyo, Japan. The reference wind speed U_H measured at the top of the models was used to calculate dynamic pressure, q_H, which was used to determine the wind pressure coefficients. The time series of pressure coefficients were filtered again by means of moving averages corresponding to

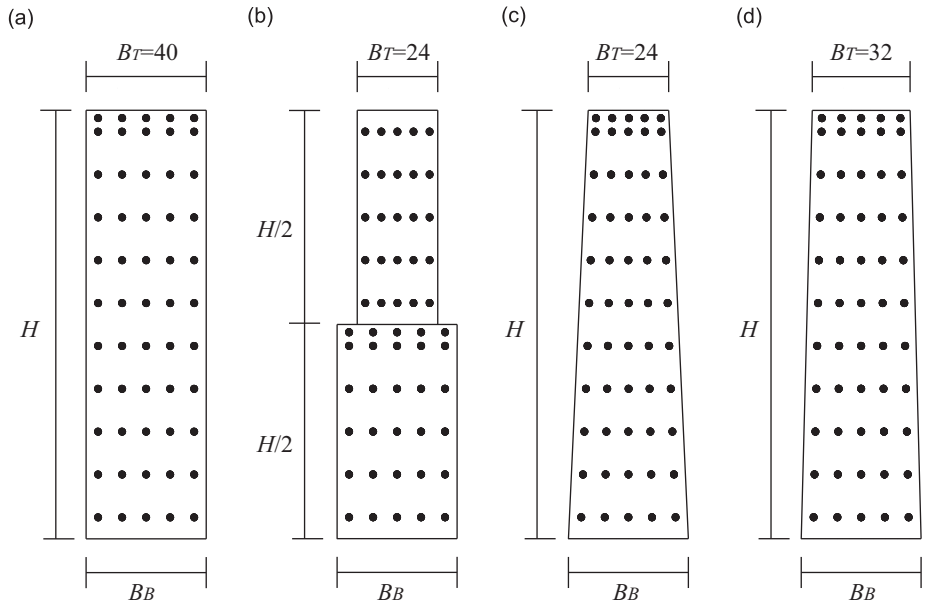

Fig. 1. Building shapes for wind tunnel test (B_B=40, H=160, unit: m). (a) SQ, (b) SB, (c) TP1 and (d) TP2.

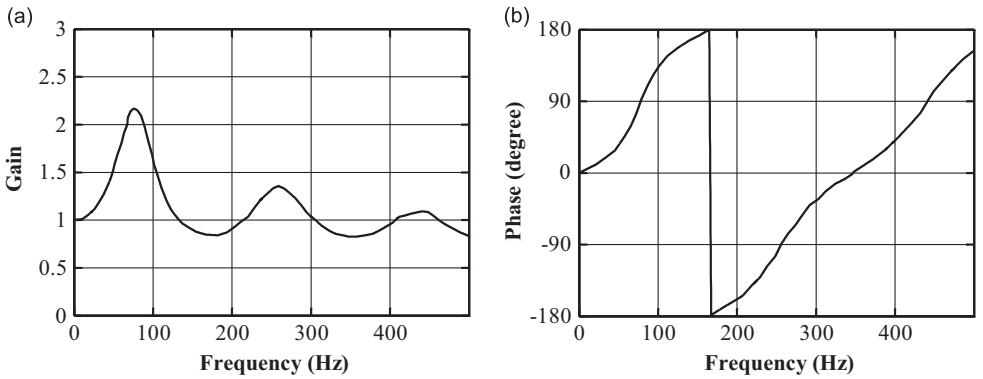

Fig. 2. Transfer functions of the tubing system. (a) Gain and (b) phase shifts.

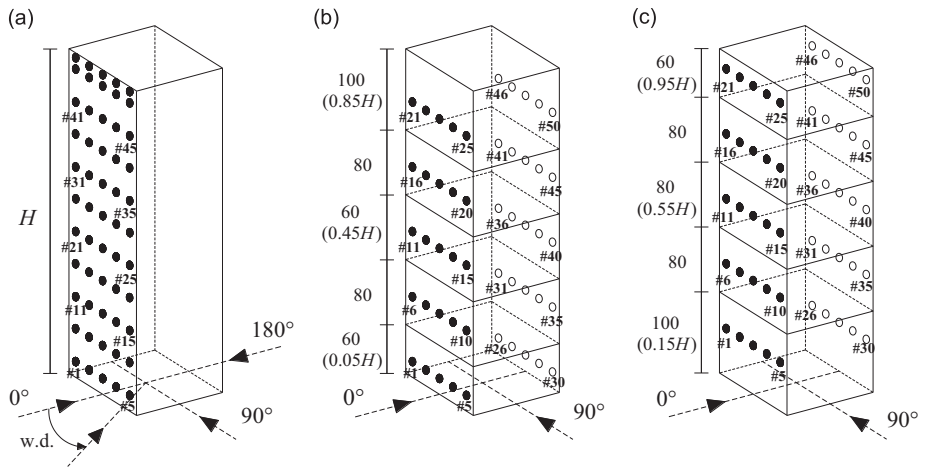

Fig. 3. Definition of wind directions and location of pressure taps (unit: mm). (a) Pressure taps on one surface, (b) pressure taps on odd level and (c) pressure taps on even level.

0.17 s for flow 1 and 0.22 s for flow 2 in full time scale using the following equation:

$$\tau = 1.0\frac{L_c}{U_H}, \tag{1}$$

where τ=moving averaging time, L_c=diagonal length of building cladding, and U_H=reference mean wind speed.

For the simulation of natural winds, two typical boundary layers were simulated: urban area flow (Flow 1, power-law exponent=0.24) with turbulence intensity at the top of the model of about 19%, and open flat area flow (Flow 2, power-law exponent=0.13) with turbulence intensity of about 15%. The profiles of mean wind speed and turbulence intensity are shown in Fig. 4(a) and (b). The thick lines indicate the equations in Recommendations for Loads on Buildings by the Architectural Institute of Japan (2004). And in Fig. 4(c), the power spectra of incident flows are presented, showing good agreement with the Karman-type spectrum. The Reynolds number was about 5.6×10^4 in flow 1 (U_H≒8.0 m/s) and about 4.5×10^4 in flow 2 (U_H≒6.5 m/s). These Reynolds numbers are lower than the full scale one by one or two orders, but as the pressures on sharp-cornered structures are adequately reproduced in the wind tunnel because the sharp corners tend to cause immediate flow separation, fixing the separation point independently of the Reynolds number of the flow (Simiu and Scanlan, 1996), it is believed that the pressures from the wind tunnel tests adequately reproduce the actual situation.

The blockage ratio was about 1.2% for a square prism, so no blockage corrections were applied to the experimental results. More detailed experimental conditions are shown in Kim and Kanda (2010a).

3. Time domain analysis

Wind pressure coefficients were calculated using the following equation:

$$C_{pi} = \frac{p_i}{0.5\rho U_H^2}, \tag{2}$$

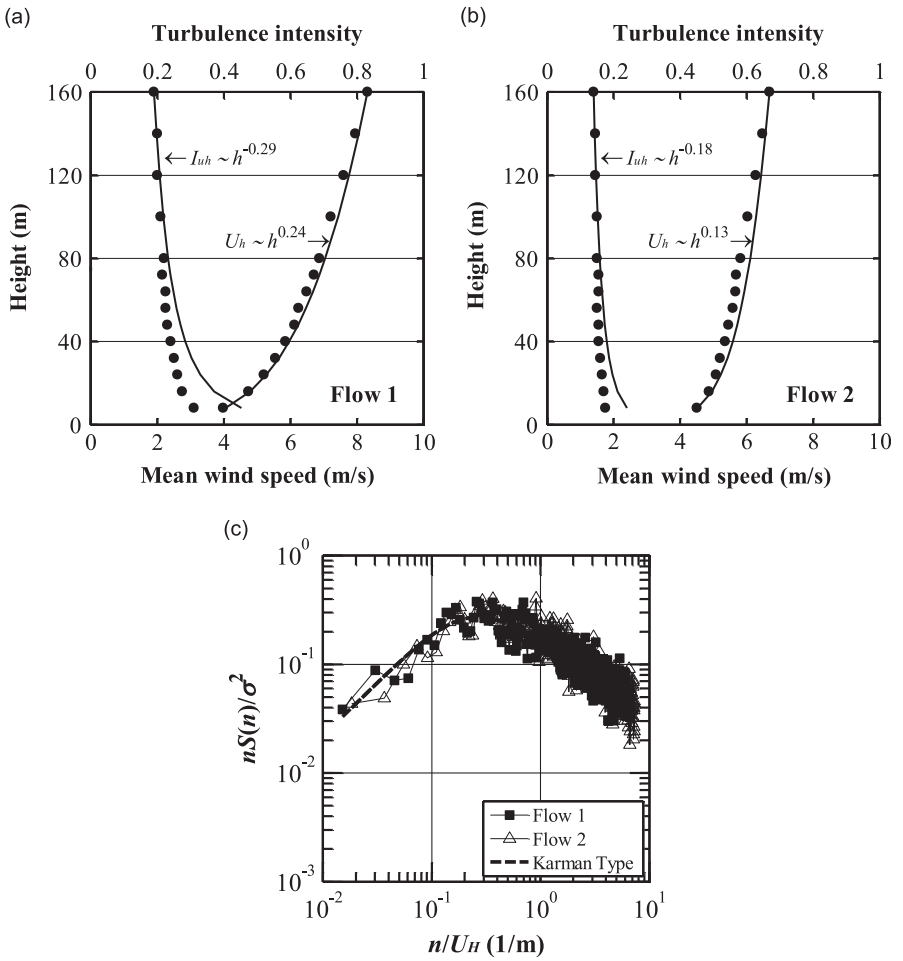

Fig. 4. Simulation of natural winds. (a) Profiles of flow 1 (urban area flow) (b) profiles of flow 2 (open flat area flow) and (c) power spectra of flow 1 and flow 2.

where p_i = mean, root mean square (r.m.s.), maximum and minimum wind pressure for one sample, and ρ = air density. The pressure coefficients are ensemble averages of 42 samples, and one sample corresponds to 10 min in full time scale.

Some differences were observed between the pressure coefficients of flow 1 and flow 2, originating from the differences in incident flows. For example, the mean pressure coefficients on the windward surface for flow 1 changed more with height than those for flow 2, due to the slope of the incident flow, and the mean pressure coefficients on the leeward surface for flow 2 were lower than those for flow 1 (larger absolute values), showing the different effect of turbulence intensity in the incident flow. In the following the main findings will be discussed.

3.1. Mean pressure coefficients

Fig. 5 shows the contours of mean pressure coefficients on windward (0°), side (90°), and leeward (180°) for flow 2. The distribution patterns of windward and side surfaces are almost the same for all models, but show slightly smaller values for the height-modified models. However, differences are found on the leeward surface. For SQ, the distribution on the leeward surface varies little, while those on the tapered and set-backed models vary largely from bottom to top, showing smaller values than SQ near the bottom and larger values near the top. This is because, for the height-modified models, the downdraft is likely to be restrained on account of increasing geometric shape with low wind speed and an up-flow is likely to be accelerated on account of decreasing geometric shape with high wind speed. For SB, it is interesting to note that there are two stagnation points on the windward surface at the lower and upper parts, respectively, and it seems that the lower and upper side surfaces are affected by the different vortex components, showing clearly separated distributions. The largest mean pressure coefficients range from 0.80 (SB) to 0.90 (SQ), at wind direction of 0°, and the smallest coefficients are −1.18 (75°) for SQ, −1.14 (75°) for the upper part of SB, −1.08 (90°) for the lower part of SB, −1.06 (75°) for TP1, and −1.14 (75°) for TP2.

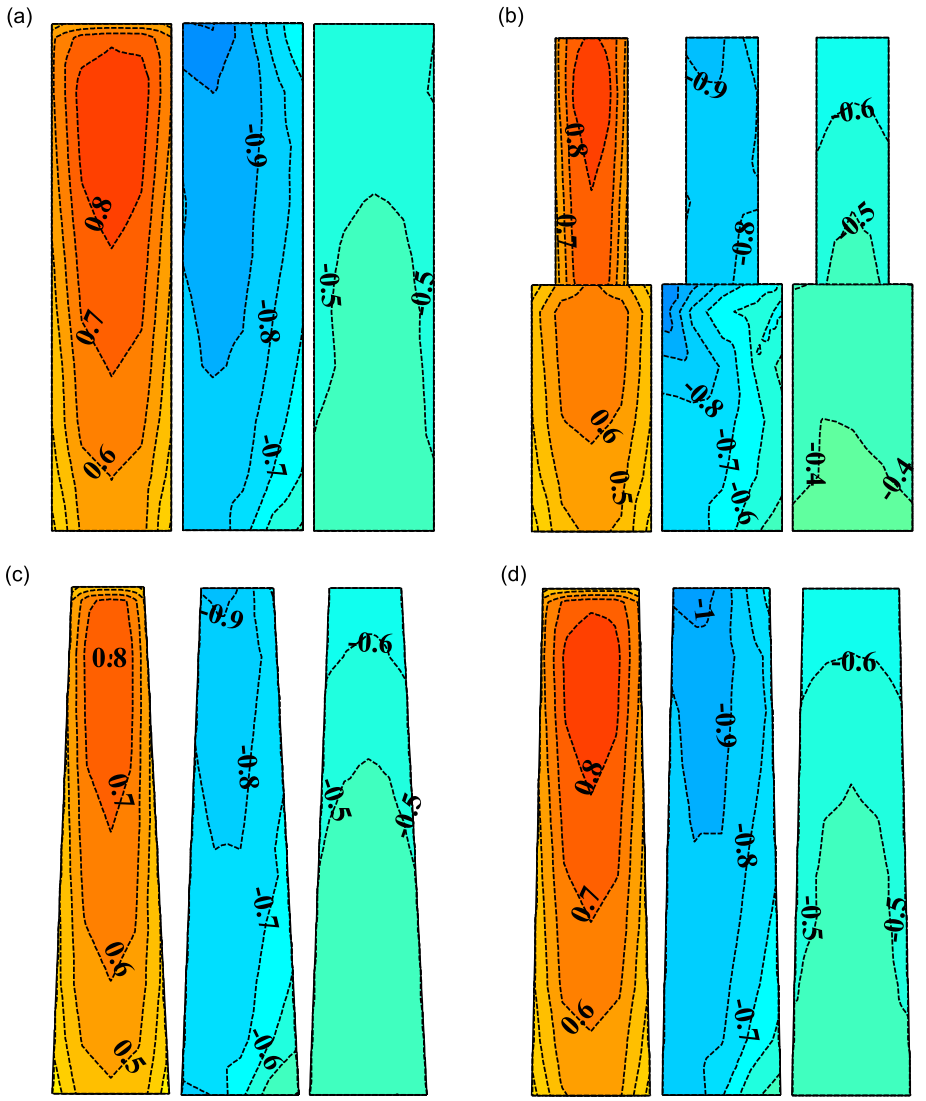

Fig. 5. Distribution of mean pressure coefficients (flow 2, from the left windward, side, and leeward surface). (a) SQ, (b) SB, (c) TP1 and (d) TP2.

The occurrence of flow reattachment at side surface can be confirmed by examining the variation of mean pressure coefficients, implying that the recovery of mean pressure coefficients indicates the occurrence of reattachment (Robertson et al., 1978). Considering this, the condition of flow reattachment was examined through the mean pressure coefficients at two heights. Variations of mean pressure coefficients at 0.05H (dotted line) and 0.85H (fine line) on the side surface are shown in Fig. 6 for flow 1 and flow 2. The abscissa indicates model depth at relevant height, and #45 is the pressure tap located at the leading edge and #41 is the tap at the trailing edge when wind flow is from left to right. For SQ, from the pressure recovery the reattachments of separated shear layers are observed at 0.05H due to the high turbulent component of the incident flow for both flows. But the pressure recovery at 0.85H near the trailing edge (#42 and #41) is larger for flow 1 than flow 2, and this implies that the degree of intermittent reattachment on the side surface is more profound for flow 1 than for flow 2 near 0.85H. For SB and TP1, although reattachments of separated shear layers occur at 0.05H in the same way as for SQ, no reattachments were found at 0.85H because of the small depth. The different flow conditions also cause smaller lift force and larger torsional moment in flow 1 than in flow 2 for all models (Kim and Kanda, 2010b).

3.2. Minimum pressure coefficients

The minimum pressure coefficients are shown in Fig. 7. They were calculated for a particular pressure tap for all wind directions employed in the present work. The smallest value (larger absolute value) was selected for the tap and the same procedure repeated for all the taps on the surface. Large negative values are observed on the upper and lower leading edge corner, and smaller values are observed on the upper and lower trailing edge corner. The asymmetric distribution is

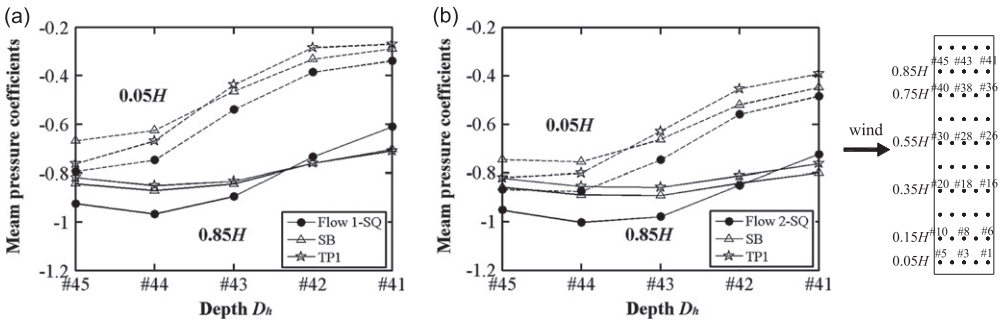

Fig. 6. Variations of mean pressure coefficients along the side surfaces at two different heights for flow 1 and flow 2 (wind is applied from the left). (a) Flow 1 and (b) flow 2.

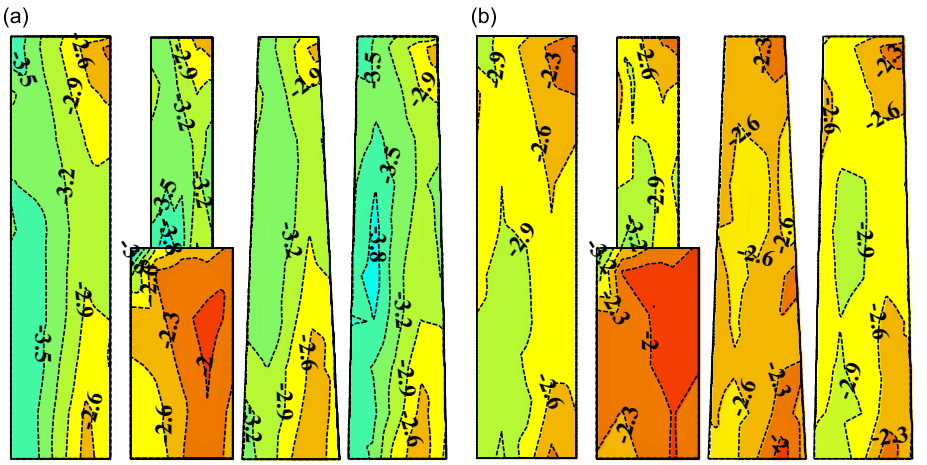

Fig. 7. Distribution of minimum pressure coefficients for flow 1 and flow 2 (from the left SQ, SB, TP1, and TP2). (a) Flow 1 and (b) flow 2.

obtained because only the results from wind direction of 0° to 180° were used. Large variations of minimum coefficients are observed on the surface for flow 1, and this large variation seems to be resulted from intermittent reattachments of separated shear layers due to high turbulence intensity as mentioned in Section 3.1. This flow condition resulted in even smaller minimum coefficients (large absolute values) for flow 1 than for flow 2. The smallest minimum coefficients are listed in Table 1, and the smallest minimum coefficients of all the models are observed for SB near the set-back as expected. It was found that most of the minimum coefficients occur when the wind direction is 90°, except for the leading edge upper corner for wind direction 75° and the trailing edge lower corner for wind directions larger than 105°.

3.3. *Cross-correlation coefficients*

Fig. 8 shows the contour of cross-correlation coefficients and fluctuating pressure coefficients of SQ, SB, and TP1 for the side surface under flow 1. The maximum values were selected and are plotted in Fig. 8(a), and their time lags, normalized using reference wind speed U_H and model bottom width B_B, are plotted in Fig. 8(b). Wind is applied from left to right, and the lowest tap on the leading edge corner marked as ● was used as the reference tap. For SQ, there are highly correlated regions in the lower leading edge corner, and the correlations gradually decrease for the direction of about 60°. Here, the time lag is found to be almost zero, and this direction also qualitatively agrees with the direction where the fluctuating coefficients show larger values, as shown in Fig. 8(c). Fluctuating pressure coefficients show the largest values on the lower leading edge corner, and also large values are observed on the upper leading and trailing edge corners. The largest time lag was observed at 0.75H, meaning that the pressure fluctuations began to occur first at 0.75H on the leading edge, and the time lag increases gradually with the parallel lines at an angle of about 60°, meaning that the pressure fluctuations were transmitted with waves inclined at an angle of 60°. Similar observations were reported by Okuda and Taniike (1990, 1993), and based on their observations, they reported the formation and shedding mechanism of an inverted conical vortex for a square prism with an aspect ratio of 4 immersed in a thinner boundary layer (boundary layer is thiner than the model height). A sketch of the qualitative mechanism of this vortex is shown in Fig. 9. At the height where the largest time lag was observed, the separated shear layer begins to roll up to form a vortex (Fig. 9(a) and (b)), and then stretches down to the bottom of the building to form the inverted conical vortex (Fig. 9(c)–(e)). As the turbulence near the floor is high and

Table 1
Minimum wind pressure coefficients for flow 1 and flow 2.

Flow	SQ	SB	TP1	TP2
Flow 1	−3.8	−4.0 (upper part) −4.3 (lower part)	−3.6	−3.9
Flow 2	−3.3	−3.4 (upper part) −3.5 (lower part)	−2.8	−3.2

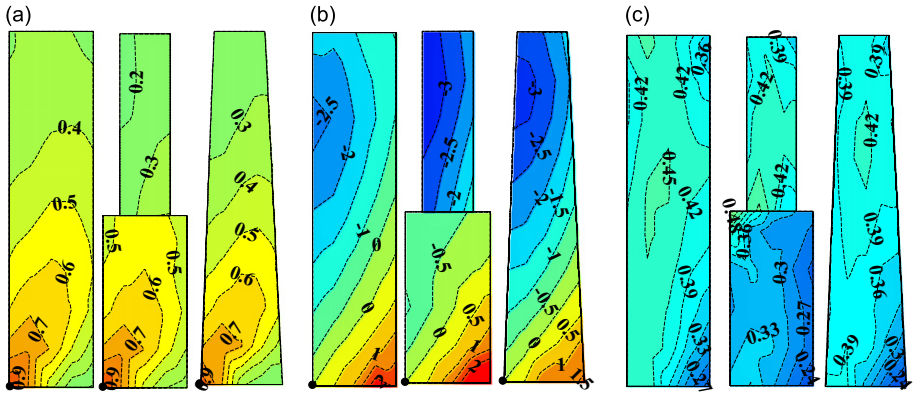

Fig. 8. Contour of maximum cross-correlation coefficients, normalized time lag and fluctuating pressure coefficients at side surfaces in flow 1 (wind is applied from the left, ● = reference point (Tap #5 in Fig. 3(a)), from the left SQ, SB, and TP1). (a) Cross-correlation coefficients, (b) normalized time lag ($\tau UH/BB$) and (c) fluctuating pressure coefficients.

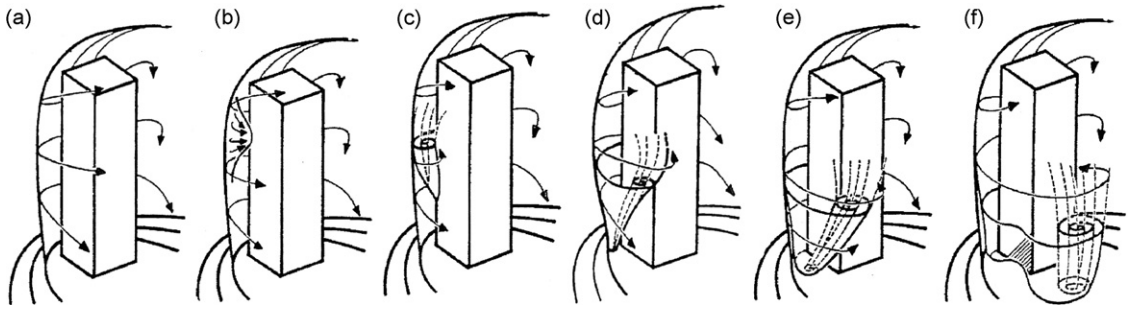

Fig. 9. Sketches of mechanism for vortex formation and shedding on square tall building (Okuda and Taniike, 1990).

this high turbulence encourages vortex formation, the core of the vortex closes to the leading edge corner as the height decreases, inducing a large peak suction at the leading edge corner on the side surface (Fig. 8(c)). Next, the vortex sheds into the wake and gradually weakens (Fig. 9(f)).

Similar patterns were found for SB and TP1, but the cross-correlation coefficients vary greatly with height, and the largest time lag is larger and is observed at a point slightly higher ($0.85H$) than SQ. The differences are very clear for SB; the cross-correlation coefficients of the lower part show similar patterns and values as the other models, but those of the upper part are very different from those of the other models and even to the lower part. Large time lag found between the upper and lower parts confirm that these parts are affected by totally different vortex components. Considering the results of Okuda and Taniike (1990, 1993), i.e., the pressure fluctuations on the side surface do not occur at the same time, and a vortex begins to form firstly at the height where the largest time lag occurs (this also means that the pressure fluctuations begin for the first time at that height), the vortex begins to roll up at a higher level for SB and TP1 than for SQ. The roll-up height is influenced by both the slope of the incident flow and the building shape. With taper and set-back, as the level where the incident flow conflicts with the leading edge is higher for SB and TP1 than for SQ, the roll-up begins at a higher level. In other words, through the taper and set-back, the height where the vortex begins to form moves up by compulsion, and as the building dimensions are small, the vortex component formed at that height sheds from the side surface more frequently or weakens before the inverted conical vortex is formed over the whole height. This also means that the shedding frequency of SB and TP1 can be higher than that of SQ at a higher level, showing height dependency of shedding frequency. The larger time lag is considered to be related somewhat to the higher shedding frequency, and because the

angle of time lag is inclined more to the downstream side for TP1, the vortexes are thought to shed at greater inclination for tapered models.

3.4. Along- and across-wind force coefficients

From the pressure measurements on opposite surfaces, wind forces were derived considering the tributary area of each tap, and the along- and across-wind force coefficients were calculated. The results for flow 1 are shown in Tables 2 and 3. Table 2 compares the along-wind force coefficients ($C_{X,\mathrm{mean}}$ and $C_{X,\mathrm{rms}}$) with the aerodynamic force measurement (Kim and Kanda, 2010b). Although there is nearly 10% error for TP2, the results match well with each other, showing slightly larger coefficients derived from wind pressures. As the errors of the two tapered models are larger than those of SQ and SB, careful consideration should be given for the determination of pressure tap position for the tapered models.

Table 3 compares the across-wind force coefficients $C_{Y,\mathrm{rms}}$. As for the along-wind force coefficients, those from the wind pressure measurement match well with those from the aerodynamic force measurement. There are little differences in the force coefficients between odd and even level.

4. Frequency domain analysis

4.1. Power spectra of pressure coefficients

As the power spectra on the windward and leeward surfaces of all the models show little difference (Kim and Kanda, 2010a), the power spectra on the side surfaces are discussed. In Fig. 10, the power spectra of wind pressure coefficients for the pressure taps located on the most upstream side at various heights (Tap #10, #20, #30 and #40 in Fig. 3(a)) for flow 1 are shown. The abscissa indicates the reduced frequency normalized by the width B_B and the reference wind speed U_H. Sharp and well aligned peaks are observed throughout the height for the reduced frequency of 0.09 for SQ, showing the largest peak at lower height. But for the height-modified models, two important observations can be made. First, the reduced frequencies for peaks (position of solid circle) vary with height, showing higher values than 0.09 with height depending on model shapes. In particular, for SB at 0.35H, there is no peak for the considered reduced frequency ranges. Second, the sharpness of the power spectra disappears and their shapes become flat. If the Strouhal number is defined as the peak reduced frequency (nB_B/U_H) in the power spectra, the Strouhal number of SQ is almost the same throughout its height (about 0.09), but for the height-modified models, it varies widely, showing increasing tendency with height. The

Table 2
Comparison of along-wind force coefficient for flow 1.

Force Coefficient	Model SQ			Model SB		
	Force	Pressure		Force	Pressure	
$C_{X,\mathrm{mean}}$	1.04	Even Odd	1.08 (1.04) 1.09 (1.05)	0.94	Even Odd	0.96 (1.02) 0.96 (1.02)
$C_{X,\mathrm{rms}}$	0.32	Even Odd	0.32 (–) 0.33 (1.03)	0.29	Even Odd	0.29 (–) 0.29 (–)
	Model TP1			Model TP2		
$C_{X,\mathrm{mean}}$	0.96	Even Odd	1.02 (1.06) 1.02 (1.06)	1.00	Even Odd	1.07 (1.07) 1.09 (1.09)
$C_{X,\mathrm{rms}}$	0.30	Even Odd	0.31 (1.03) 0.31 (1.03)	0.31	Even Odd	0.33 (1.06) 0.33 (1.06)

Table 3
Comparison of across-wind force coefficient for flow 1.

Force Coefficient	Model SQ			Model SB		
	Force	Pressure		Force	Pressure	
$C_{Y,\mathrm{rms}}$	0.33	Even Odd	0.33 (–) 0.34 (1.03)	0.22	Even Odd	0.20 (0.91) 0.21 (0.95)
	Model TP1			Model TP2		
$C_{Y,\mathrm{rms}}$	0.26	Even Odd	0.27 (1.04) 0.27 (1.04)	0.30	Even Odd	0.31 (1.03) 031 (1.03)

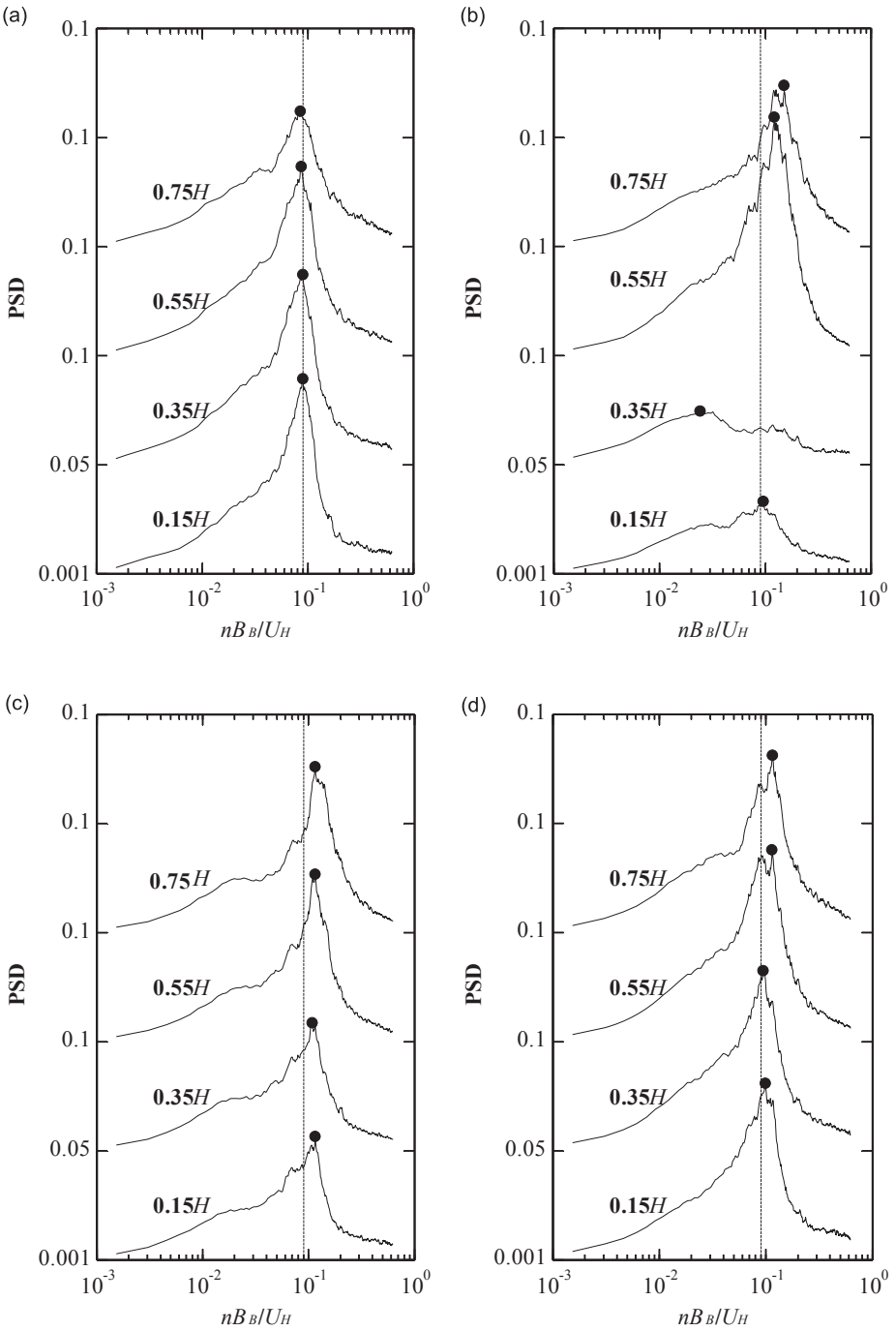

Fig. 10. Power spectra of pressure coefficients at various heights for flow 1 using the most upstream pressure taps on side surface (tap # 10 (0.15H), tap # 20, tap # 30, and tap # 40 (0.75H) in Fig. 3(a)). (a) SQ, (b) SB, (c) TP1 and (d) TP2.

shedding frequencies are controlled by the Strouhal number in terms of the width B_B. If the width is not constant, vortices cannot be formed and shed regularly throughout the height, dividing the model into small independent cells, each shedding weaker vortices. For the height-modified models, as the width decreases, the shedding frequency increases with height, and the related process was demonstrated in Section 3.3 in terms of cross-correlation coefficients and time lag.

Fig. 11 shows detailed comparisons of spectral peaks of all models at 0.75H and 0.15H for flow 1 and flow 2 using the same taps as shown in Fig. 10. At lower height (Fig. 11(a) and (c)), the peak of SQ is the largest among all the models, showing larger values than TP2, TP1 and SB in that order. However, the peaks of the height-modified models at upper height (Fig. 11(b)) for flow 1 are larger than that of SQ. This is quite an interesting result, and the heights where the power

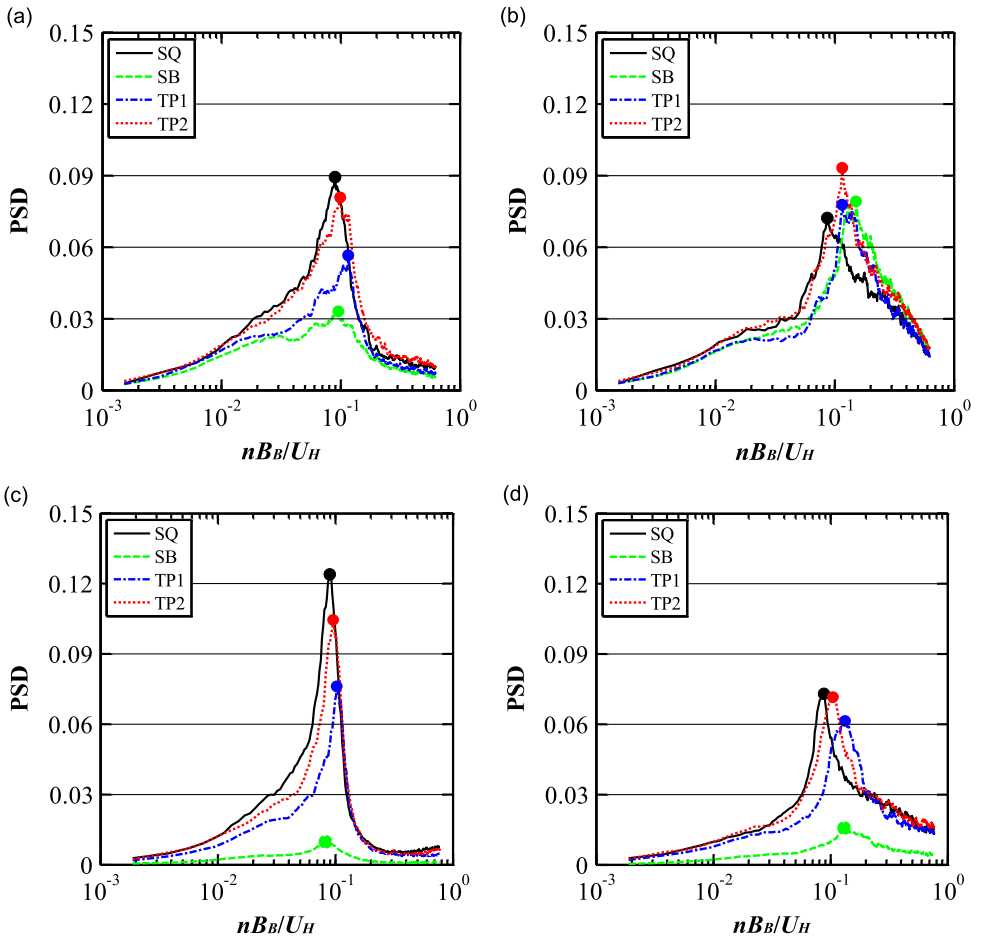

Fig. 11. Comparison of power spectra of pressure coefficients at various heights on side surface for flow 1 and flow 2. (a) 0.15H for flow 1 (Tap #10 in Fig. 3(a)), (b) 0.75H for flow 1 (Tap #40 in Fig. 3(a)), (c) 0.15H for flow 2 (tap #10 in Fig. 3(a)) and (d) 0.75H for flow 2 (Tap #40 in Fig. 3(a)).

of SQ is the smallest are shown by the hatched area in Fig. 12. A power higher than SQ was observed roughly at heights above 0.6H, and this result is only observed for flow 1. From the variation of mean pressure coefficients in Fig. 6, it can be imagined that intermittent attachments occur on the side surface of SQ for flow 1 but not for the other models, and this difference in flow condition is considered to be responsible for these results.

4.2. Spanwise and chordwise co-coherences on one surface

Co-coherences of wind pressure coefficients on the windward (0° in the legend) and leeward (180° in the legend) surfaces for flow 2 are shown in Fig. 13. Co-coherence was defined as real part of the cross-spectral density, i.e., coincident spectral density, being normalized by the product of the two power spectra, which can be negative values depending on the two positions. Fig. 13(a) shows the spanwise co-coherences for the taps along the center line (0.75H (tap #38)–0.15H (tap #8)) and Fig. 13(b) shows those for the taps along the side line (0.75H (tap #36)–0.15H (tap #6)). The abscissa indicates the reduced frequencies normalized by the geometric mean of width at two heights B_{hm} and reference wind speed U_H. The dotted line indicates the wind speed co-coherence proposed by Kim and Kanda (2010a), which is given by

$$C_{12}(r_y,r_z,n) = \exp(-r^* \cdot n^*), \tag{3}$$

where $r^* = \sqrt{(k_y r_y)^2 + (k_z r_z)^2}/L_{x,zm}$ is the normalized distance, the $n^* = \sqrt{1+(nL_{x,zm}/k_2\overline{U}_{zm})^2}$ normalized frequency, the k_y, k_z, k_2 constants determined by wind tunnel test, the r_y, r_z distances between two points, the L_x turbulence scale, the z_m geometric mean of two points.

Eq. (3) was proposed in the form of exponential function using a normalized distance and normalized frequency term considering that the co-coherences on windward and leeward surfaces decrease monotonically. k_y, k_z, and k_2 were determined using wind tunnel test results, and set to $k_y = k_z = 0.5$, and $k_2 = 0.05$–0.07 depending on distance. In Fig. 13, $k_2 = 0.05$ was used. Eq. (3) was compared with wind tunnel data measured at various heights in two boundary layers and full-scale data for points 40 m apart horizontally and 40 m above the ground, and 10 m apart vertically and 10 m above the

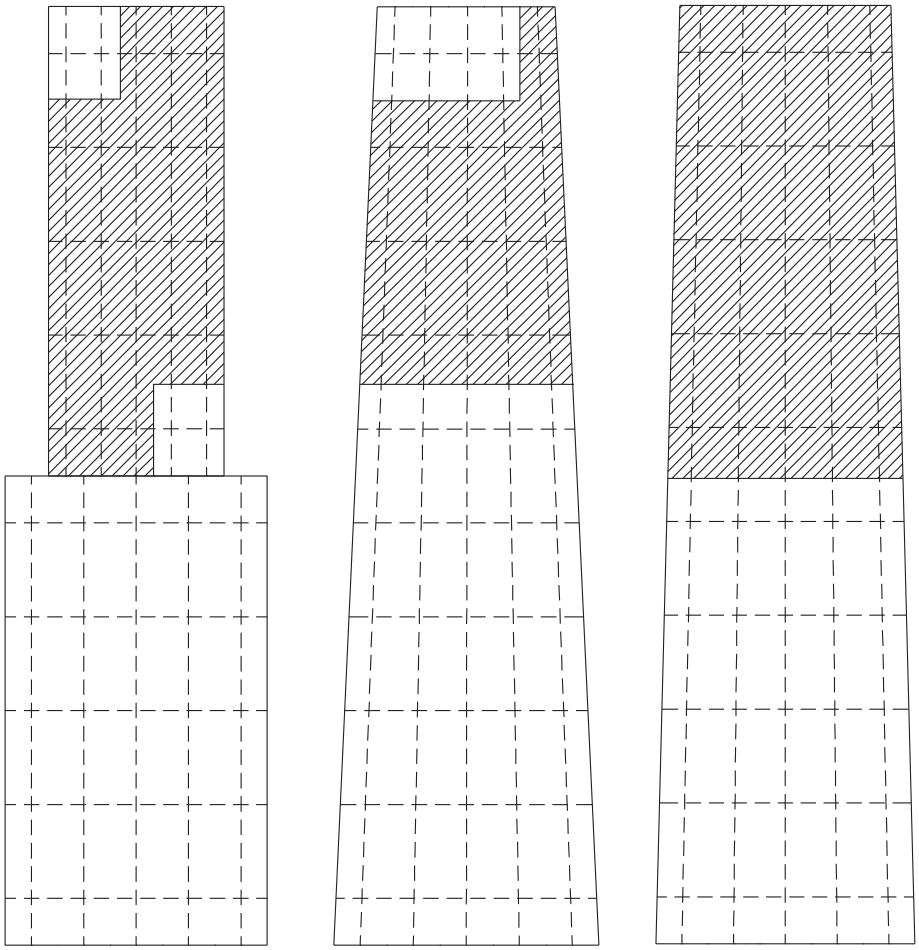

Fig. 12. Model heights with higher spectral peak values than SQ on side surface for flow 1 (Wind is applied from the left, From the left SB, TP1 and TP2).

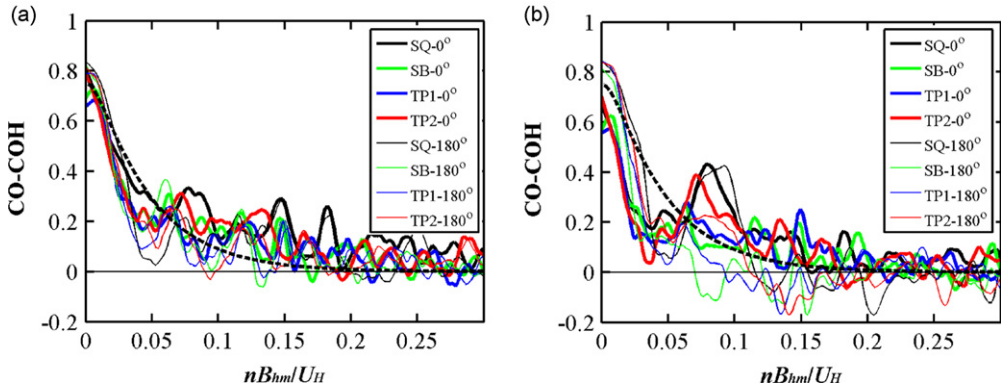

Fig. 13. Spanwise co-coherences of pressure coefficients on windward and leeward surfaces between 0.75*H* and 0.15*H* for flow 2. (a) Center line taps (tap #38–tap #8 in Fig. 3(a)) (b) Side line taps (tap #36–tap #6 in Fig. 3(a))

ground, showing good agreements. The differences among models in the spanwise co-coherences shown in Fig. 13 are very small regardless of tap positions, and the spanwise co-coherences generally match well with Eq. (3), meaning that the wind pressure co-coherences on the windward and leeward surfaces can be expressed by the same equation as the wind speed co-coherences. Note that in the spanwise co-coherences of side line taps (Fig. 13(b)), there is a clear peak near the reduced frequency of 0.1 in windward and leeward surfaces for SQ.

The spanwise co-coherences on the side surface are shown in Fig. 14 for flow 1 and flow 2 using pressure taps located at the most upstream side (0.75*H* (tap #40)–0.55*H* (tap #30) and 0.75*H* (tap #40)–0.15*H* (tap #10)). The effect of higher

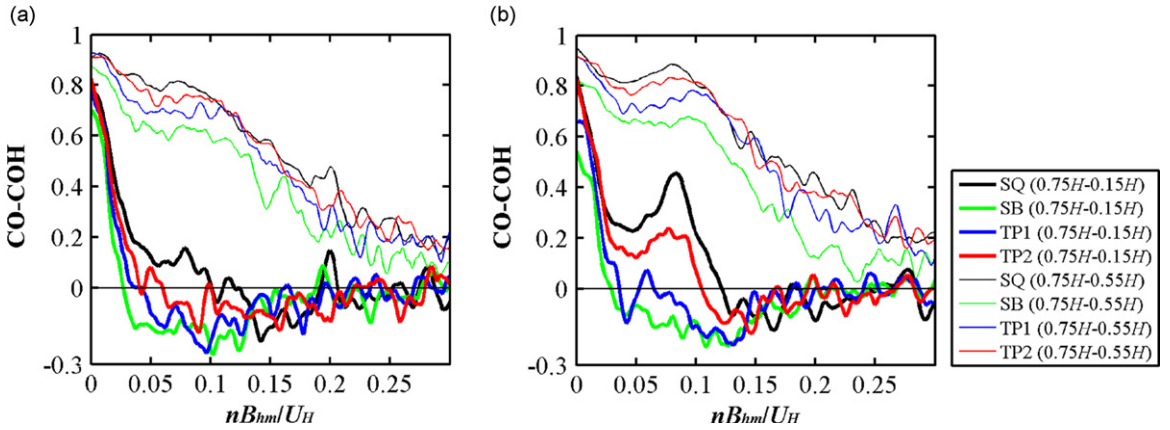

Fig. 14. Spanwise co-coherences of pressure coefficients on side surfaces for flow 1 and flow 2 (0.75*H* (tap #40)–0.55*H* (tap #30), and 0.75*H* (tap #40)–0.15*H* (tap #10) in Fig. 3(a)). (a) Co-coherence for flow 1 and (b) co-coherence for flow 2. (For interpretation of the references to color in this figure caption, the reader is referred to the web version of this article.)

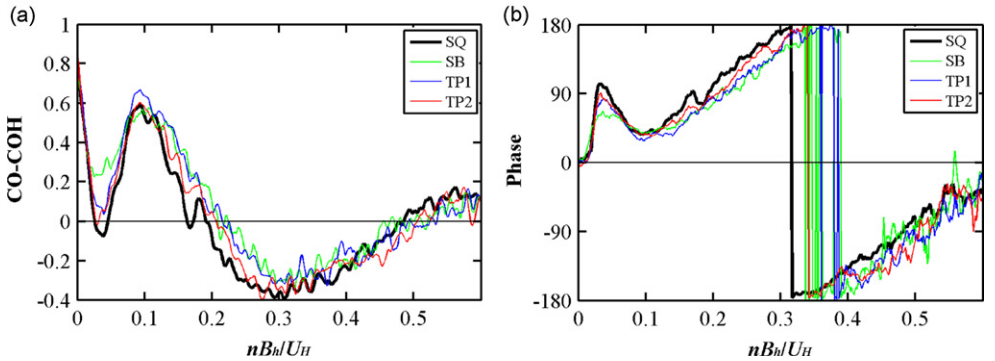

Fig. 15. Chordwise co-coherences and phase of pressure coefficients on side surfaces for flow 2 (0.75*H*, tap #40–tap #36 in Fig. 3(a)). (a) Co-coherence and (b) phase

turbulence intensity can again be observed: i.e., the peak near the reduced frequency of 0.1 is sharper for flow 2 than for flow 1. Focusing on the results of flow 2 (Fig. 14(b)), high correlations are observed near the reduced frequency of 0.1 for all models between 0.75*H* and 0.55*H*. A clear peak near reduced frequency 0.1 is observed for correlation between 0.75*H* and 0.15*H* for SQ. But for the tapered models, as the tapering ratio increases, the peak near reduced frequency 0.1 decreases gradually and when the tapering ratio is 10% (blue line) a small negative peak is observed. This is also observed for SB. Similar trends can be observed for the results of flow 1, although only a small peak is observed even for SQ. For flow 1, although the spectral peaks of the height-modified models are larger than that of SQ for heights above 0.6*H* (Fig. 12), as the co-coherences among heights is much smaller than for SQ as shown in Fig. 14(a), it was found that the peaks of the across-wind force power spectra of the height-modified models are smaller than that of SQ (Kim and Kanda, 2010a).

The co-coherences and phases of pressure taps at 0.75*H* between the most upstream side tap (Tap #40) and the most downstream side tap (Tap #36) are shown in Fig. 15 for flow 2. For all models, peaks near reduced frequency 0.1 are clearly observed and the co-coherence becomes negative near reduced frequency 0.2, showing the smallest co-coherence near reduced frequencies 0.3. The co-coherence becomes nearly zero after 0.6. The correlations of the height-modified models are slightly higher in the ranges from 0.1 to 0.4 than that for SQ, but the differences after that become very small. In the reduced frequency ranges for the negative co-coherences, the phase becomes larger than $+90^\circ$ or smaller than -90° (out of phase). The phase at reduced frequency 0.1 is about 35°, and at reduced frequencies 0.2 and 0.5, where the co-coherence is almost zero, the phase is nearly $\pm 90^\circ$. The co-coherences at lower levels show peaks near reduced frequency 0.1, but no negative co-coherences are observed, and the co-coherences become zero at a relatively low reduced frequency of about 0.2. In flow 1, similar tendencies were observed, although the peak becomes quite small and flat due to the higher turbulence intensity.

4.3. Spanwise co-coherences on opposite surfaces

Spanwise co-coherences between windward and leeward pressure taps are shown in Fig. 16 for flow 1. The reference tap of the odd level is tap # 25 (0.85*H*), which is located along the side line, and the reference tap of the even level is tap # 18 (0.75*H*), which is located along the center line shown in Fig. 3(b) and (c). Although high co-coherences are observed in

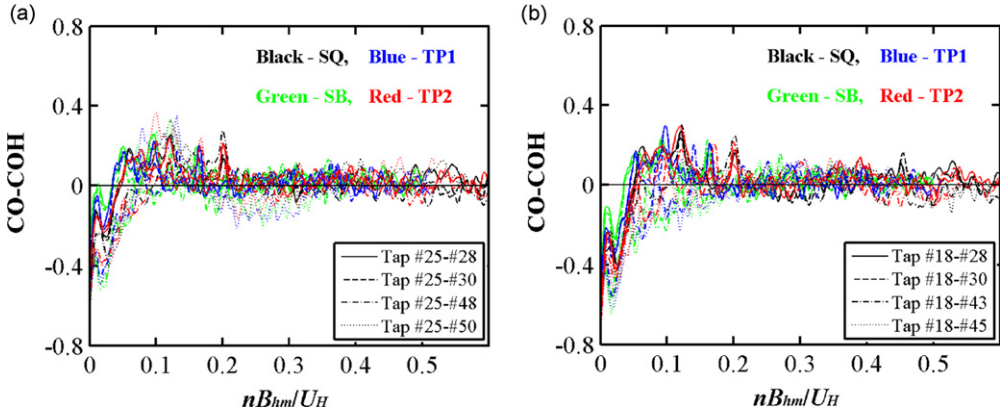

Fig. 16. Co-coherence between windward and leeward pressure taps for flow 1. (a) Odd level (For tap number, see Fig. 3(b)) and (b) even level (For tap number, see Fig. 3(c))

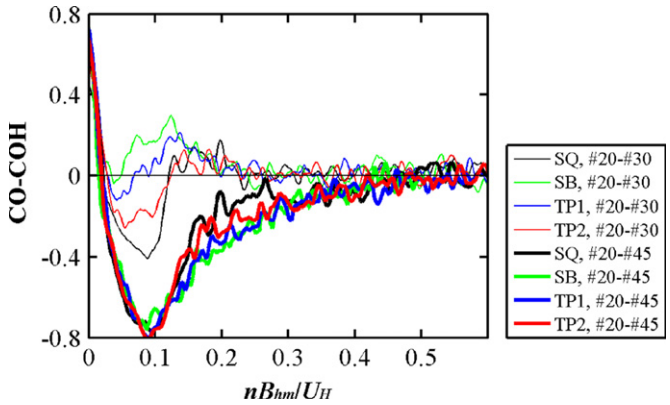

Fig. 17. Co-coherence between opposite side pressure taps for flow 2 (even level, Fig. 3(c)).

low frequency ranges (lower than 0.05), the co-coherences between windward and leeward surfaces can be said to be generally low regardless of building shape and pressure tap positions. The correlations between windward and leeward surfaces have been one of the most important factors in the evaluation of gust factor, which has been studied since the 1960s (Davenport, 1967; Simiu, 1973, 1983; Vickery, 1970). Davenport (1967) and Vickery (1970) assumed that the windward and leeward surfaces are fully correlated. However, Simiu (1973, 1983) pointed out that the coherence is very low, 0–0.2, from the results of wind tunnel tests and full scale measurement. Besides these researchers, many others (Kao, 1971; Lam Put, 1971; Tamura et al., 1996; Von Koten, 1974) also reported the correlation to be low, and so far the fact that low or no correlation between windward and leeward surfaces is well recognized. In the present study, this is again confirmed even for the height-modified models, and the constant correlation of 0.1 ($\gamma=0.1$) is used for the evaluation of along-wind force power spectra shown below.

Fig. 17 shows the spanwise co-coherence of pressure taps located on opposite side surfaces (90°). The reference tap is tap #20 at 0.75H and dummy taps are tap #45 (0.75H) and tap # 30 (0.15H) on the opposite side surface as shown in Fig. 3(c). For SQ (fine and thick black line), negative peaks near the reduced frequency of 0.1 are clearly shown regardless of tap distances, and the peak for the upper level taps are more significant (Tap #20–Tap #45). As the tap distances increase (Tap #20–Tap #30), although the peak near 0.1 is shown, the correlation abruptly becomes zero right after the reduced frequency of 0.1. Large differences among models are found in the correlations between 0.75H and 0.15H (Tap #20–Tap #30). As the taper ratio increases, the negative peak near the reduced frequency of 0.1 decreases, and for SB and TP1, a positive peak is observed. This shows the inverse correlations between the two heights, as previously shown in Fig. 14(b). The reduced frequencies where the correlation becomes zero are higher in the height-modified models than SQ.

4.4. Along- and across-wind power spectra

The along-wind force power spectrum was calculated numerically using the wind speed co-coherence in Eq. (3). The along-wind force power spectrum can be expressed as Eq. (4), once the following assumptions are made: there are no eccentricities on mass and rigidity, profile of mean wind speed follows the power law, and the standard deviation and

power spectrum of fluctuating wind speed is constant with height represented as $S_{u,H}$:

$$S_F(n) = 4\left(\frac{1}{2}\rho U_H^2 BHC_D^*\right)^2 \frac{S_{u,H}}{U_H^2}$$

$$\int_0^1\int_0^1\int_0^1\int_0^1 {z_1}^{\alpha+m}{z_2}^{\alpha+m}\exp\left(-\sqrt{1+\left(\frac{nL_{x,zm}}{k_2\overline{U}_{zm}}\right)^2}\cdot\frac{\sqrt{(k_y r_y B)^2+(k_z r_z H)^2}}{L_{x,zm}}\right)dy_1\,dy_2\,dz_1\,dz_2, \tag{4}$$

where $C_D^* = \sqrt{C_{p_w}^2 - 2\gamma C_{p_w}C_{p_L} + C_{p_L}^2}$, $S_{u,H}$ is the wind speed power spectrum at model height (constant with height), y_1, y_2, z_1, and z_2 is the horizontal and vertical coordinates, α is the power law exponent for mean wind speed, m is the power law exponent for mode shape. The 4th order integral can be reduced to a 2nd order integral using appropriate operations of the inner two integral terms by introducing the influence function (Dyrbye and Hansen, 1996). The final form of the along-wind power spectrum for shear force ($m=0$ in Eq. (4)) becomes

$$S_F(n) \cong 4\left(\frac{1}{2}\rho U_H^2 BHC_D^*\right)^2 \frac{S_{u,H}}{U_H^2}$$

$$\int_0^1\int_0^1 2(1-r_y)(1-r_z)^{2\alpha}\left\{r_z+\frac{2(1-r_z)}{2\alpha+1}\right\}\exp\left(-\sqrt{1+\left(\frac{nL_{x,zm}}{k_2\overline{U}_{zm}}\right)^2}\cdot\frac{\sqrt{(k_y r_y B)^2+(k_z r_z H)^2}}{L_{x,zm}}\right)dr_y dr_z. \tag{5}$$

Note that the variables in Eq. (4) are y_1, y_2, z_1, and z_2, but those in Eq. (5) are distances between two points in each direction (r_y ($=y_1-y_2$), and r_z ($=z_1-z_2$)).

Fig. 18 compares the three power spectra normalized by their variances. The black line indicates the normalized power spectrum obtained by aerodynamic force measurement (Kim and Kanda, 2010b) and the red line indicates the normalized power spectrum by wind pressure measurement. And, the normalized power spectrum from Eq. (5) is shown by a green dotted line. For all models, the power spectra show good agreements for the wide reduced frequency ranges, although a

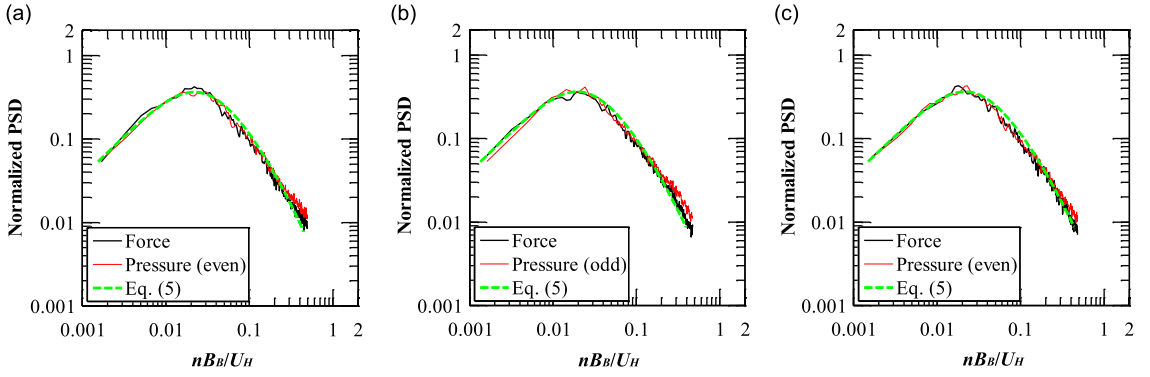

Fig. 18. Comparison of normalized along-wind power spectra for flow 1. (a) SQ, (b) SB, and (c) TP1. (For interpretation of the references to color in this figure caption, the reader is referred to the web version of this article.)

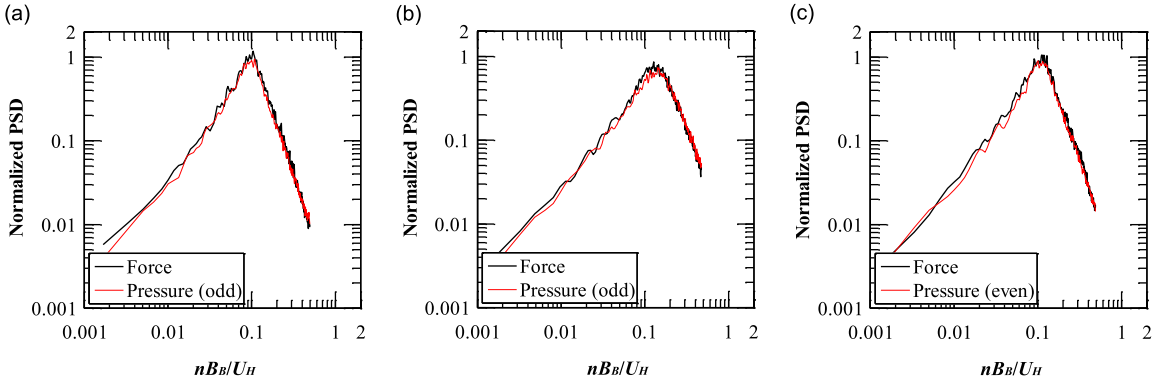

Fig. 19. Comparison of normalized across-wind power spectra for flow 1. (a) SQ, (b) SB, and (c) TP2

little discrepancy is shown between red line and other two lines for reduced frequencies higher than 0.3. In the calculation of Eq. (5), the correlation between windward and leeward surfaces (γ) was set to 0.1, and the pressure coefficients defined at each height, not model height, were used.

Comparison of normalized across-wind power spectra derived from aerodynamic force measurement (Kim and Kanda, 2010b) and from pressure measurement is shown in Fig. 19. The two power spectra correspond very well for the wide reduced frequency ranges, including the peaks near the reduced frequency of 0.1.

5. Conclusions

Through a series of wind pressure measurements on height-modified models, the following conclusions were drawn.

(i) While the mean pressure coefficients on the windward surfaces of all the models are almost the same, those on the leeward surfaces are clearly different. For example, in flow 2, mean pressure coefficients of SQ on the leeward surface is about -0.5, whereas for SB those range from about 0.4 near the bottom to about 0.6 near the top. These differences are caused by the geometric characteristics of the models.

(ii) The minimum pressure coefficient of SB is smaller than that of SQ (larger absolute value), and occurs near the set-back zone. In flow 1, the minimum pressure coefficient of SQ is -3.8 and that of SB is -4.3, and in flow 2, those are -3.3 and -3.5, respectively.

(iii) The effect of different flow conditions on reattachment on a side surface is examined from the variation of mean pressure coefficients and power spectral peaks. And different flow conditions also affect on the minimum coefficients: the absolute values of minimum coefficients in flow 1 are larger than those of flow 2.

(iv) Vortex formation and shedding mechanisms of taper and set-back models were discussed. For the height-modified models, the maximum cross-correlation coefficients vary widely with height, showing smaller values at higher levels than SQ (less than 0.3). And the largest time lag is larger and is observed at a higher level than SQ. For SQ, the largest time lag is found at $0.75H$, while those of the height-modified models are $0.85H$. This means that the vortex on the side surface begins to form at higher levels for the height-modified models.

Aerodynamic modifications through taper and set-back affect on the bandwidth of power spectra and position of peak frequencies in the spanwise direction. The effects of different peak frequencies are clearly observed by the co-coherences of wind pressures applied to the same and opposite side surfaces. For SQ, a regular vortex shedding occurs through all levels, but by changing the building shapes the height of vortex formation moves upward by compulsion, and due to the small dimension at upper levels the vortex sheds more frequently than at lower levels, disturbing vortex formation throughout the height, and making vortex shedding random and incoherent with height.

Reference

Architectural Institution of Japan, 2004. Recommendations for Loads on Buildings. Architectural Institution of Japan, Tokyo.

Davenport, A.G., 1967. Gust loading factor, ASCE. Journal of the Structural Division 93, 11–34.

Dutton, R., Isyumov, N., 1990. Reduction of tall building motion by aerodynamic treatments. Journal of Wind Engineering and Industrial Aerodynamics 36, 739–747.

Dyrbye, C., Hansen, S.O., 1996. Wind Loads on Structures. John Wiley & Sons, pp. 207–209.

Hui, Y., Yoshida, A., Tamura, Y., 2013. Interference effects between two rectangular-section high-rise buildings on local peak pressure coefficients. Journal of Fluids and Structures 37, 120–133.

〈http://www.skyscrapercenter.com/List/future-tallest-100-buildings〉 (Last access: 2012/12/15).

Iungo, G.V., Pii, L.M., Buresti, G., 2012. Experimental investigation on the aerodynamic loads and wake flow features of a low aspect-ratio circular cylinder. Journal of Fluids and Structures 28, 279–291.

Kao, K.H., 1971. Measurements of Pressure/Velocity Correlation on a Rectangular Prism in Turbulent Flow, Engineering Science Research Robert BLWT-2-20. University of Western Ontario, London, Canada.

Kareem, A., Cermak, J.E., 1984. Pressure fluctuations on a square building model in boundary-layer flows. Journal of Wind Engineering and Industrial Aerodynamics 16, 17–41.

Kawai, H., 1998. Effect of corner modifications on aeroelastic instabilities of tall buildings. Journal of Wind Engineering and Industrial Aerodynamics 74–76, 719–729.

Kim, Y.C., Kanda, J., 2010a. Characteristics of aerodynamic forces and pressures on square plan buildings with height variations. Journal of Wind Engineering and Industrial Aerodynamics 98 (8-9), 449–465.

Kim, Y.C., Kanda, J., 2010b. Effects of taper and setback on wind force and wind-induced response of tall buildings. Wind and Structures 13 (6), 499–517.

Kim, Y.C., Kanda, J., Tamura, Y., 2011. Wind-induced coupled motion of tall buildings with varying square plan with height. Journal of Wind Engineering and Industrial Aerodynamics 99 (5), 638–650.

Kwok, K.C.S., Wilhelm, P.A., Wilkie, B.G., 1988. Effect of edge configuration on wind-induced response of tall buildings. Engineering Structures 10, 135–140.

Lam Put, R., 1971, Dynamic response of tall building to random wind loads, in: Proceeding of the Third International Conference on Wind Effects on Buildings and Structures, Tokyo, Saikon Shuppan, pp. 429–440.

Lin, N., Letchford, C., Tamura, Y., Liang, B., Nakamura, O., 2005. Characteristics of wind forces acting on tall buildings. Journal of Wind Engineering and Industrial Aerodynamics 93 (3), 217–242.

Okuda, Y., Taniike, Y., 1990. On the flow and pressure fields around a three dimensional prism, part 2. Annuals of Disaster Prevention Research Institute B-1 (33), 297–308. in Japanese.

Okuda, Y., Taniike, Y., 1993. Conical vortices over side face of a three-dimensional square prism. Journal of Wind Engineering and Industrial Aerodynamics 50, 163–172.
Robertson, J.M., Wedding, J.B., Peterka, J.A., Cermak, J.E., 1978. Wall pressures of separation – reattachment flow on a square prism in uniform flow. Journal of Wind Engineering and Industrial Aerodynamics 2 (4), 345–359.
Simiu, E., 1973. Gust factors and alongwind pressure correlations, ASCE. Journal of the Structural Division 99, 773–783.
Simiu, E., 1983. Modern development in wind engineering: part 4. Engineering Structures 5, 273–281.
Simiu, E., Scanlan, R.H., 1996. Wind Effects on Structures: Fundamentals and Applications to Design, third ed. John Wiley & Sons, Inc., pp. 297–298.
Tamura, Y., Kawai, H., Uematsu, Y., Marukawa, H., Fujii, K., Taniike, Y., 1996. Wind load and wind-induced response estimations in the recommendations for loads on buildings, AIJ, 1993. Engineering Structures 18, 399–411.
Tanaka, H., Tamura, Y., Ohtake, K., Nakai, M., Kim, Y.C., 2012. Experimental investigation of aerodynamic forces and wind pressures acting on tall buildings with various unconventional configurations. Journal of Wind Engineering and Industrial Aerodynamics 107-108, 179–191.
Vickery, B.J., 1970. On the reliability of gust loading factors, Proceeding of Technical Meeting Wind Loads on Buildings and Structures. National Bureau of Standards, Washington, pp. 93–104.
Von Koten, H., 1974, The fluctuating wind pressures on the cladding and inside a building, in: Proceedings of Symposium on Full Scale Measurements of Wind Effects on Tall buildings, The University of Western Ontario, pp. 23–29.